14th World Congress in Computational Mechanics (WCCM)
ECCOMAS Congress 2020
Virtual Congress: 11 – 15 January 2021
F. Chinesta, R. Abgrall, O. Allix and M. Kaliske (Eds)

# A SIMPLIFIED BLADE MODEL FOR RELIABLE SEISMIC ASSESSMENTS OF WIND TURBINES

**AHMER ALI[1], RAFFAELE DE RISI[1]**

[1] University of Bristol
University Walk, Queen's Building, BS8 1TR, Bristol, UK
ahmer.ali@bristol.ac.uk, raffaele.derisi@bristol.ac.uk

**Keywords:** Genetic algorithm, Optimisation, Dynamic analysis.

**Abstract.** Wind turbines are dynamically complex structures. They entail slender towers, flexible foundations, and heavy rotor-nacelle-assembly (RNA). In the context of earthquake analysis, the RNA is often simplified as a rigid point mass which can suppress the modal contribution of blades from the global system dynamics and may further affect the reliability of seismic response of wind turbines. Other high-fidelity finite element (FE) blade models are difficult to implement due to the complex layup of composite materials and reduced computational efficiency. Thus, there is a need for an intermediate solution that allows the realistic and accurate consideration of blades in the seismic assessment of wind turbines. This study presents a meta-heuristic, problem-independent optimisation method, known as the genetic algorithm (GA), to identify simplified material and cross-sectional properties of a typical wind turbine blade. The properties are used to construct a simplified FE blade model that can be implemented in global wind turbine models. The optimised design solutions are examined with regards to the mechanical and dynamic response of a reference 5MW wind turbine having 61.5 m long blades. The accuracy of the modal behaviour validates the presented optimisation and simplified blade modelling approach and signifies the potential of its application in seismic assessments of wind turbines.

## 1 INTRODUCTION

With new offshore wind farms being planned in earthquake-prone regions, there is a rising interest in investigating the seismic vulnerability of wind turbines. In this context, numerical models utilized for dynamic analysis of wind turbines idealise or even oversimplify the rotor details [1–6]. The general details on a rotor-nacelle-assembly (RNA), such as the rotor diameter, nacelle, hub, and the blades' mass, are readily available [7–9] and are simple to model. However, the local blades details, such as airfoil shape, twist angle, and material distribution, are not only challenging to find but are also numerically complicated and computationally expensive. As a result, it is a common practice to either assume these details [5–7,10] and/or use the lumped mass approach to represent the RNA in finite element models (FEM) of wind turbines [1,11].

Some of the most detailed information in the literature is provided by the National Renewable Energy Laboratory (NREL) that entails the detailed structural specifications of a 5MW wind turbine developed for research purposes [8]. Their report comprehensively described the size, shape, mass, and stiffness distribution of not only the tower, nacelle, hub but also the blades. However, it lacked the description of materials, local cross-sectional details, and methods used to calculate the blade properties. Several studies have reported the design and optimisation of composite blades using complex FE shell or solid element models to evaluate their strength and modal response [12–15]. Such high-fidelity FE models are difficult to implement with reasonable computational efficiency in earthquake engineering problems, particularly when a large number of numerical analyses of the whole rotor-tower-foundation-system is needed under a representative set of earthquake records [1,7,10,11].

Hence, there is a need for an intermediate solution that allows the realistic consideration of the blades in the earthquake-specific numerical assessments of wind turbines. This study presents an FE integrated genetic algorithm (GA) based blade optimisation. GA is a problem-independent optimisation method, proven to robustly solve complex eigenvalue problems [16], optimise wind turbine tower performance [3], composite blade shapes [24,25], and wind farm layouts [26–28]. The objective function is defined in terms of blade mass and its location, moment of inertia, and frequencies (flapwise and edgewise). Six optimisation variables are considered, including (1) cross-sectional thickness ($t$), (2) thickness gradient along the blade ($S$), (3) material density ($\rho$), (4,5) Young's modulus of a uniform but anisotropic material ($E_y$ and $E_z$), and (6) shear modulus ($G$). The optimised blade design solutions are used to develop the FE blade model and assess its mechanical and dynamic characteristics with respect to the NREL reference 5MW/61.5 m blade. The optimised blade is also implemented in the 5MW wind turbine model to signify its efficacy and discuss the influence of local blade modes on the global system dynamics.



## 2 GENETIC ALGORITHM-BASED BLADE OPTIMISATION

Genetic algorithms (GA) are meta-heuristic, non-deterministic optimisation procedures following the principles of natural selection and genetics [17,18]. A GA is an evolutionary process, starting upon a random set of individuals in a population, iteratively improved by genetic modification to acquire the optimised solution of the problem. In this study, a finite element (FE) integrated GA is employed to optimise the mass, stiffness, and modal response of a wind turbine blade. The mechanical and dynamic characteristics of the 61.5 m blade from the 5MW NREL reference wind turbine is used as the target. These are termed constraint conditions ($C_{i,T}$), as shown in Table 1. The aim is to determine the mechanical and modal properties that are representative of realistic wind turbine blades. The objective function ($F_{obj}$) is defined using Equation (1 – 2). It assesses the accuracy of the optimised blade properties ($C_{i,E}$) and evaluates their difference with the target constraints ($C_{i,T}$).

$$F_{obj} = \min\left(E_{global}\right) \tag{1}$$

$$E_{global} = \left(\sum_{i=1}^{n}\left|1 - \frac{C_{i,E}}{C_{i,T}}\right|\right)/n\,; \quad \text{where, } n = 7 \tag{2}$$

**Table 1:** Constraint conditions ($C_{i,T}$)

| Constraint Definition | | | Symbols | | NREL [8] FAST | NREL [8] ADAMS | Units |
|---|---|---|---|---|---|---|---|
| Mass | | | $m$ | $C_1$ | 17,740 | | kg |
| Centre of mass | | | $CM$ | $C_2$ | 20.475 | | m |
| Mass moment of inertia | 1st | | $Q$ | $C_3$ | 363,231 | | kg.m |
| | 2nd | | $I_m$ | $C_4$ | 11,776,047 | | kg.m$^2$ |
| Modal frequency | Flapwise | 1st | $f_{1F}$ | $C_5$ | 0.666 | 0.629 | Hz |
| | | 2nd | $f_{2F}$ | $C_6$ | 1.922 | 1.651 | |
| | Edgewise | 1st | $f_{1E}$ | $C_7$ | 1.079 | 1.074 | |

The blade FEM is calibrated considering six design variables as listed in Table 2. Each optimised design solution ($\lambda_j$) will be a vector of candidate design variables, which is referred to as a chromosome in a GA, where '$n$' design variables represent its genes, as expressed in Equation (3).

$$\lambda_j = [\lambda_1\ \lambda_2 \ldots \lambda_n],\ \ n = 6 \tag{3}$$

**Table 2**: Constraint ranges of the design variables

| Design Variable Definition | Symbol | | Upper bound | Lower Bound | Units |
|---|---|---|---|---|---|
| Thickness | ($t$) | $\lambda_1$ | 15 | 35 | mm |
| Gradient | ($S$) | $\lambda_2$ | 1 | 4 | $\times 10^{-4}$ |
| Material density | ($\rho$) | $\lambda_3$ | 1220 | 1920 | kg/m$^3$ |
| Young's modulus | ($E_y$) | $\lambda_4$ | 40 | 115 | GPa |
| | ($E_z$) | $\lambda_5$ | 8 | 14 | |
| Shear modulus | ($G$) | $\lambda_6$ | 2 | 12 | |

The thickness ($t$), its gradient ($S$) and material density ($\rho$) will control the mass, whereas Young's moduli ($E_y$, $E_z$) and shear modulus ($G$) will influence the stiffness across the blade span. The upper and lower bound of design variables are constrained to reflect the material properties (such as Carbon, Foam, Gelcoat, Saertex) commonly used in the composite layup of a typical wind turbine blade [14,19]. A more detailed material can be used for the structural design of the shear webs, the spar caps, core, upper and lower composite laminates of the blade [20,21]. However, this is beyond the present scope as the goal is to obtain an optimised solution, in terms of $\lambda_j$ considered in Table 2, that can yield the target mass, stiffness, and modal response regardless of the blade configurations, i.e., with or without webs, structural twist, etc.

Figure 1 shows the blade optimisation procedure followed by the FEA integrated GA implemented using MATLAB in this study [22]. The key algorithm parameters include the definition of problem constraints (Table 1), variables (Table 2), objectives (Equation (1 – 2)), convergence control and stopping criteria. A population size of 200 individuals is initially used by random selection. The blade modal analysis is performed using the individuals (candidate design solutions) and optimised blade properties are monitored ($C_{i,E}$) following the fitness/objective function ($F_{obj}$). The individuals with the best mean fitness are passed on to the next generation of populations, while those with the worst fitness are eliminated from the population sampling. The maximum number of generations and the iterations per generation control the convergence speed, taken as $100 \times n$ and 50, respectively [3]. The fitness function and constraint tolerance control the accuracy, set as $10^{-6}$ and $10^{-3}$, respectively. The number of iterations and continual recurrence of minimum fitness value over the generations compose the GA stopping criteria. The algorithm parameters may need to be redefined in case of unsatisfactory convergence of an optimised design solution (DS).

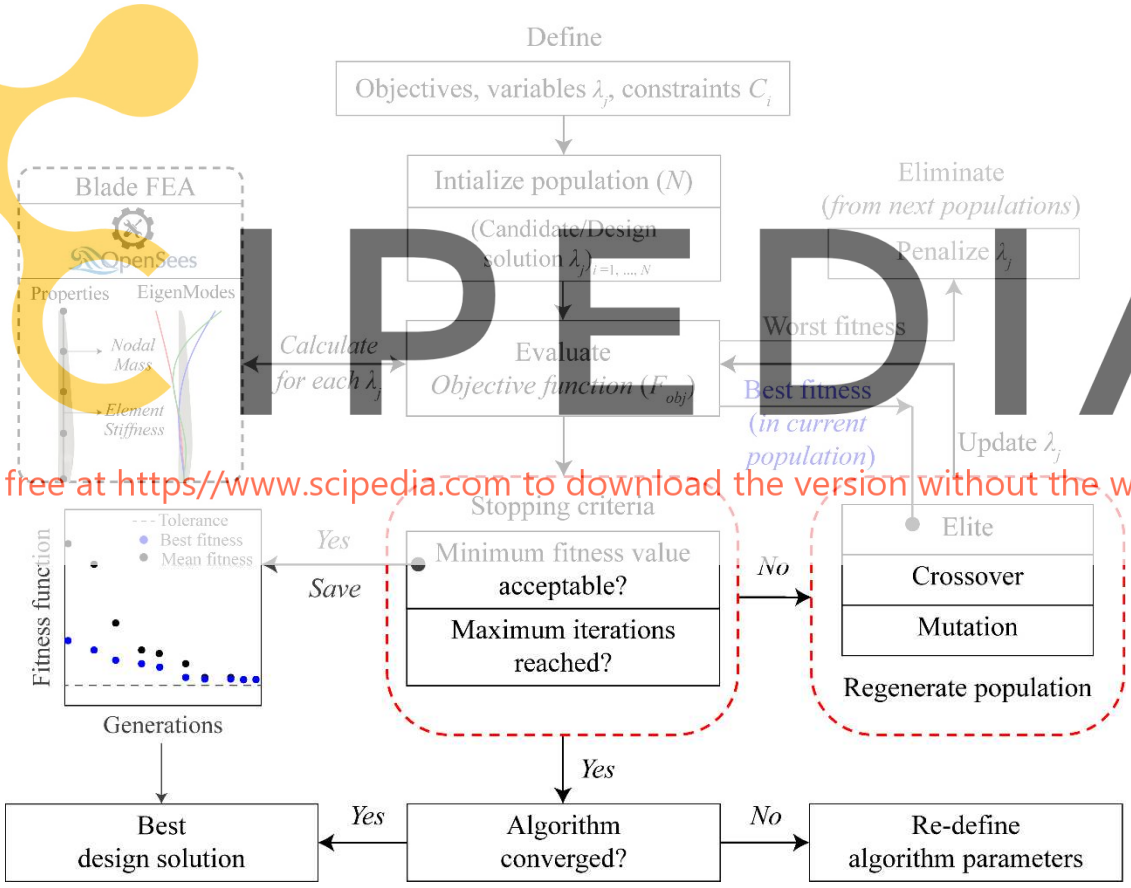


**Figure 1:** Flowchart of the FE-integrated GA procedure for blade optimisation

## 3 BLADE FEM

The FEM of the 61.5 m fixed root blade is modelled using elastic beam-column elements in OpenSees software [23]. This element type requires simpler material and cross-sectional

definition, and it is often used for nonlinear seismic assessment of wind turbine towers due to computational efficiency [7,10]. The airfoil area ($A$) and moments of inertia ($I_x$, $I_y$, $I_z$) are used to define the cross-sectional properties, whereas density ($\rho$), Young's modulus ($E$) and shear modulus ($G$) are employed for material definition. The airfoil cross-sectional properties are estimated following the relations provided by Ali et al. [24], for which the optimised blade thickness and its variation across the span are used. Similarly, optimised $\rho$, $E$, and $G$ are used to calculate the FE blade element stiffnesses in the flapwise, edgewise and torsional directions.

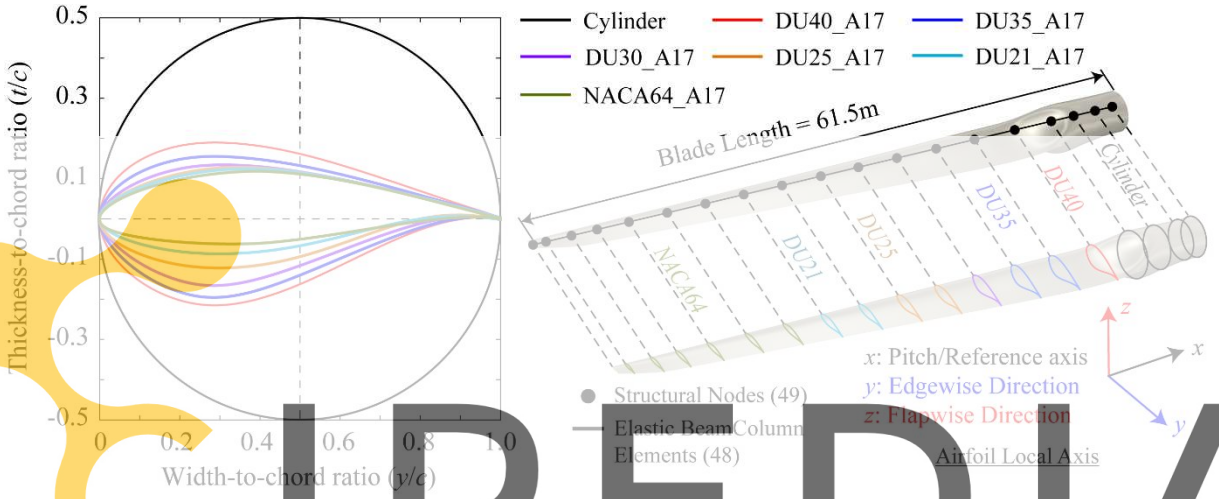


**Figure 2:** (a) Airfoil shapes, (b) FEM of the 61.5 m blade developed in OpenSees



Figure 2 shows the shape and distribution of the airfoils used across the blade span. The blade is divided by 49 nodes into 48 elements, similar to discretization used in the NREL 5MW blade [8]. It may be noted that the wind turbines are generally stiffened by shear webs and have a varying structural twist and pitch axis location [8,14]. It would affect the nodal mass and element stiffness. This study investigates the effects of pitch axis location on the optimised DS in achieving the target mechanical and modal blade response. Two pitch axis locations are assumed for the blade, (1) at the centroid of the airfoils and (2) at their elastic centre, measured from the leading edge of each airfoil. For the first case, the pitch axis is assumed to be located at $y/c$ =0.275 for non-circular airfoil shapes and 0.5 for circular shapes, which is almost equivalent to their centroidal locations [14]. For the second case, the pitch axis is assumed to pass the airfoils at $y/c$ = 0.25, following Jonkman et al. [8], where $c$ is the chord length of each airfoil. It is important to emphasise that the presented GA-based FE optimisation is also applicable to other blade configurations, i.e., those with webs and structural twists. However, their details are omitted here for brevity and are comprehensively discussed elsewhere [24].

## 4 RESULTS

Figure 3 shows the progression of the fitness function at each generation. The blue points and the line show the mean fitness function value at each generation, whereas the data in black reflects the fitness of the best design solution (DS) within a generation. The GA tends to minimize the global objective function ($E_{global}$) through the sequence of generations until an entire population converges at the lowest possible value, resulting in a unique DS. For both pitch axis locations, GA converges at around 100 generations approximately. However, the best fitness value is lower for the blade where the pitch axis passes through its elastic centre, as shown in Figure 3(b). This implies the optimised DS for this case will be closer to the target blade properties and the dynamic response. This is shown in Table 3 and Table 4, where the former described the optimised values of the six design variables used in this study, and the latter shows the resulting blade properties and modal frequencies.

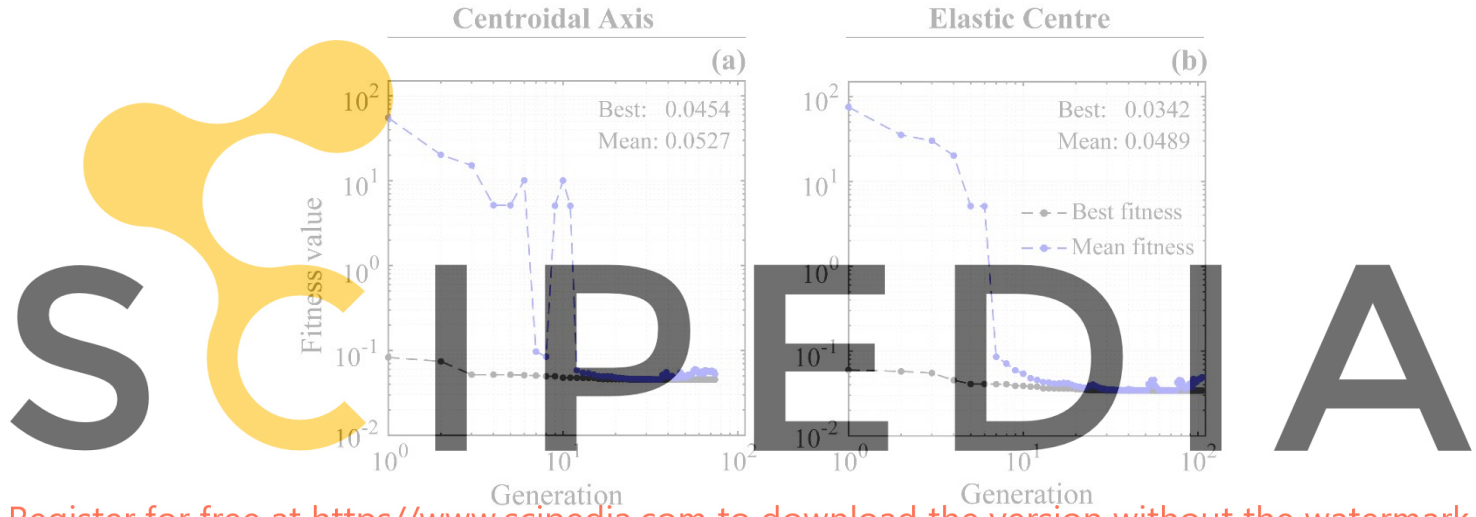




**Figure 3:** Progression of the fitness function for GA based blade optimisation

**Table 3:** Optimised design solution (DS) of the blade

| Design solution (DS) | | | Blade pitch axis | | Units |
|---|---|---|---|---|---|
| Variable | Symbol | | Centroidal axis | Elastic centre | |
| | | | DS-1 | DS-2 | |
| Thickness | ($t$) | $\lambda_1$ | 26.62 | 26.80 | mm |
| Gradient | ($S$) | $\lambda_2$ | 3.08 | 3.16 | $\times 10^{-4}$ |
| Density | ($\rho$) | $\lambda_3$ | 1872 | 1893 | kg/m$^3$ |
| Young's modulus | ($E_y$) | $\lambda_4$ | 40.02 | 40.01 | GPa |
| | ($E_z$) | $\lambda_5$ | 13.99 | 9.20 | |
| Shear modulus | ($G$) | $\lambda_6$ | 5.69 | 6.05 | |

It can be observed that the GA resulted in unique solutions for both blade configurations, shown in Table 3 and termed as DS-1, and DS-2. It is plausible to achieve a different combination of optimised variables, as GA follows a stochastic random process for candidate selections within a population. Despite their difference, all DS must result in blade properties and modal response identical to the target. This is shown in Table 4, where the undistributed blade properties resulting from the two optimised DS are presented. The term 'undistributed' refers to the overall blade properties rather than at each cross-section (termed as 'distributed' herein). It is shown that for both DS, the blade's mass, its locations, the moment of inertia and flapwise and edgewise frequency are in good agreement with the target values. The efficiency of the solution is further examined at the blade's cross-sections.

**Table 4:** Blade frequencies and undistributed properties obtained using the optimised DS

| Parameter | | Mass | Centre of mass | Moment of inertia | | Modal frequency | | |
|---|---|---|---|---|---|---|---|---|
| | | | | 1st | 2nd | Flapwise | | Edgewise |
| Symbol | | $(m)$ | $(CM)$ | $(Q)$ | $(I_m)$ | $(f_{1F})$ | $(f_{2F})$ | $(f_{1E})$ |
| | | $C_1$ | $C_2$ | $C_3$ | $C_4$ | $C_5$ | $C_6$ | $C_7$ |
| Units | | kg | m | kg.m | kg.m$^2$ | Hz | | |
| NREL(FAST) | | 17,740 | 20.475 | 363,231 | 11,776,047 | 0.666 | 1.922 | 1.079 |
| Estimated | DS-1 | 17,100 | 21.291 | 364,084 | 11,776,047 | 0.689 | 2.089 | 0.971 |
| | DS-2 | 17,272 | 21.172 | 365,678 | 11,776,047 | 0.698 | 2.120 | 1.079 |



Figure 4 shows the change in blade mass density, flapwise stiffness and edgewise stiffness along the blade span ($L$). The structural properties are shown along the normalised blade length ($\Delta l/L$) as compared to the NREL blade [8]. The blade mass densities for both solutions are mutually identical with the target (Figure 4 (a)). Similarly, flapwise and edgewise stiffnesses, shown in Figure 4(b) and (c), are generally in good agreement with the NREL blade; however, there is slight overestimation and underestimation of the stiffness near the blade root, respectively.

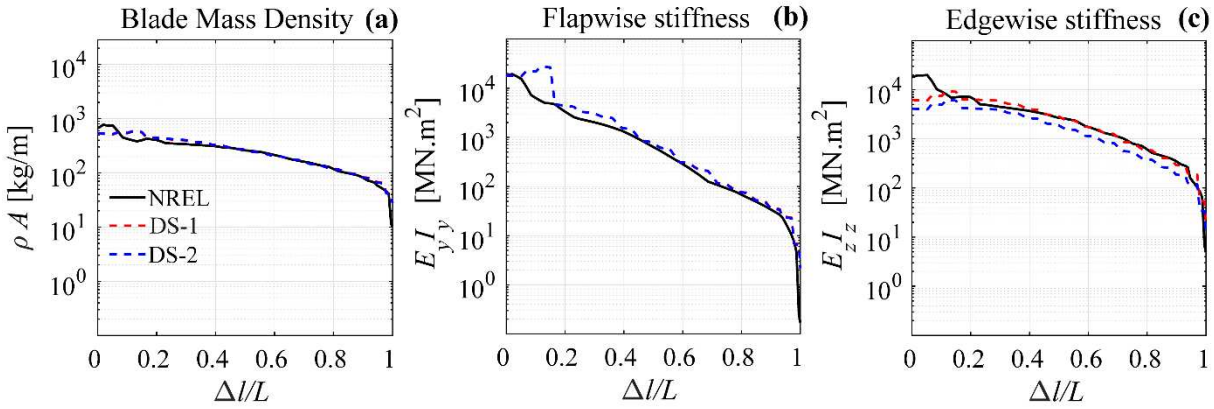


**Figure 4:** Distributed structural properties of the blade with varying pitch axis locations

### 4.1 Dynamic response of the blade

The dynamic response of the blade is examined using the active modal masses and mode shapes, shown in Figure 5. The first three purely translational flapwise ($U_X$) and edgewise ($U_Y$) mode shapes and their participation mass (PM) distribution is shown for the blades with varying pitch axis location, i.e., at the airfoils' centroid (DS-1) and their elastic centre (DS-2). The distribution of the active masses is nearly identical for both solutions, inferring the efficiency of the simplified blade FE modelling solutions provided in this work. However, it takes around 40 to 50 modes to achieve 90% PM in X, Y, and Z directions. This indicates a prominent higher mode behaviour due to the blade's complex geometry, varying structural mass and stiffness along its length. In general, rotor-nacelle-assembly (RNA) is idealised as the lumped point mass atop the tower, considering the RNA intrinsically rigid and ignoring the effects of local blade modes on the global system dynamics. This can be crucial for reliable seismic assessment of wind turbines at both onshore and offshore locations.



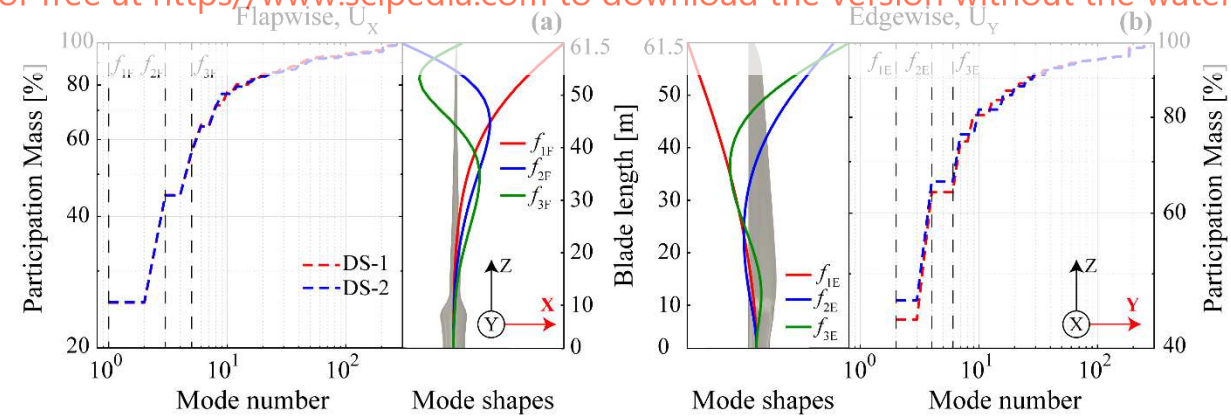


**Figure 5:** Mode shapes and participation masses of blades with varying pitch axis location

### 4.2 Dynamic response of a 5MW wind turbine

The optimised blades are implemented in the numerical modelling of the NREL 5MW

land-based wind turbine in OpenSees [23]. Like blades, the 87.6 m high tower is developed using beam-column elements. The hub and nacelle are represented by point masses at their respective centre of mass locations. Rigid links are used for connecting blades-to-hub-to nacelle and tower with the RNA. More details on the approach used for structural modelling of the wind turbine can be found in [7,10,25]. The blade properties are used following DS-1, presented in Table 3. Eigenvalue analysis is performed for the fixed base wind turbine considering the two blade configurations. Figure 6 shows the first six eigenmodes capturing the first-order tower and blade modes and their vibration periods ($T$) which are in good agreement with the reference wind turbine [8]. It may be noted that mode 4 to 6 are related to the flapwise and edgewise modes, indicating higher mode behaviour in wind turbines which is neglected using the conventional lumped mass approach [1]. Thus, it can be concluded that the presented simplified FE model is efficient in representing the realistic dynamic behaviour of blades which should be considered for reliable seismic assessment of wind turbines.

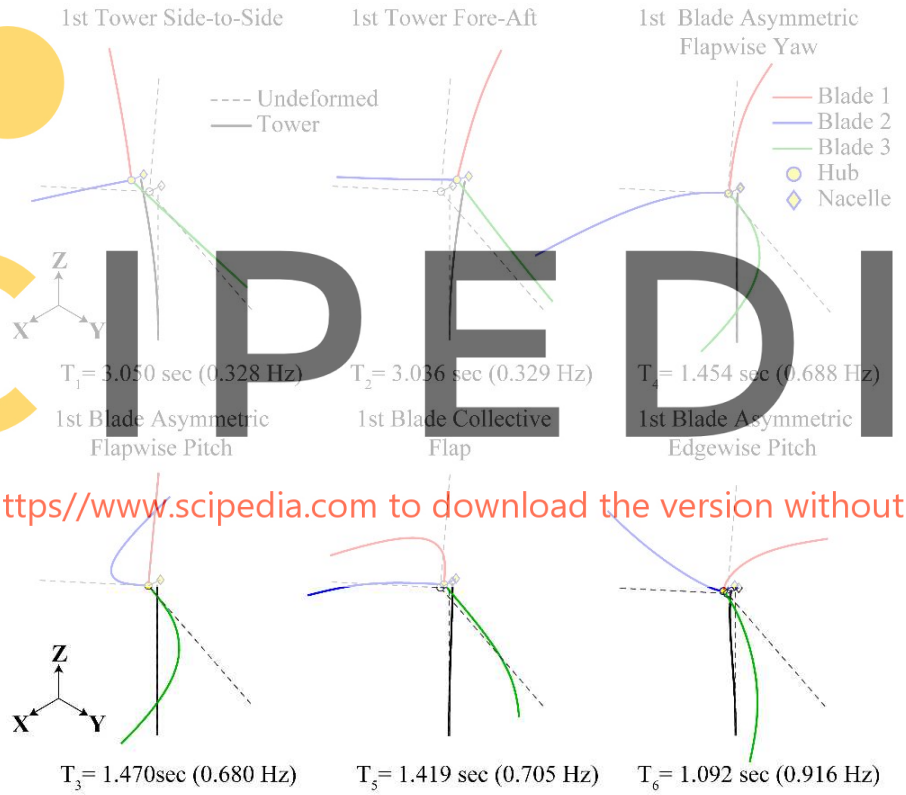




**Figure 6:** First-order tower and blade mode shapes and vibration periods

## 5 CONCLUSIONS

Structural analysis is crucial for the seismic vulnerability assessment of wind turbines. The rotor-nacelle-assembly (RNA) is often idealised as a lumped mass to avoid blades' complexity. This study presents a genetic algorithm (GA) based optimisation of wind turbine

blades for their simplified yet realistic implementation in global finite element (FE) models of wind turbines. The conclusions drawn from this study are as follows.

- The FE integrated GA provided unique design solutions (DS) for each blade configuration.
- Each DS resulted in identical blade properties and dynamic response, indicating the efficiency of the optimisation procedure and the simplified blade model presented in this work.
- The optimised blade mass, flapwise and edgewise moment of inertia, stiffnesses, and frequencies are in good agreement with the target constraints.
- The modal analysis revealed activation of higher blade modes that can contribute to higher mode response in both onshore and offshore wind turbines. The conventional lumped mass approach ignores the local blade modes' effects which may lead to unreliable seismic numerical assessments of wind turbines.

## REFERENCES


1. Sadowski AJ, Camara A, Málaga-Chuquitaype C, Dai K. Seismic analysis of a tall metal wind turbine support tower with realistic geometric imperfections. *Earthquake Engineering & Structural Dynamics* 2017; **46**(2): 201–219.
2. Alati N, Failla G, Arena F. Seismic analysis of offshore wind turbines on bottom-fixed support structures. *Phil Trans R Soc A* 2015; **373**(2035): 20140086.
3. Gentils T, Wang L, Kolios A. Integrated structural optimisation of offshore wind turbine support structures based on finite element analysis and genetic algorithm. *Applied Energy* 2017; **199**: 187–204.
4. Patil A, Jung S, Kwon OS. Structural performance of a parked wind turbine tower subjected to strong ground motions. *Engineering Structures* 2016; **120**: 92–102.
5. Zhao Z, Dai K, Lalonde ER, Meng J, Li B, Ding Z, *et al.* Studies on application of scissor-jack braced viscous damper system in wind turbines under seismic and wind loads. *Engineering Structures* 2019; **196**: 109294.
6. Martín del Campo JO, Pozos-Estrada A. Multi-hazard fragility analysis for a wind turbine support structure: An application to the Southwest of Mexico. *Engineering Structures* 2020; **209**: 109929.
7. De Risi R, Bhattacharya S, Goda K. Seismic performance assessment of monopile-supported offshore wind turbines using unscaled natural earthquake records. *Soil Dynamics and Earthquake Engineering* 2018; **109**: 154–172.
8. Jonkman J, Butterfield S, Musial W, Scott G. Definition of a 5-MW Reference Wind Turbine for Offshore System Development 2009(February).
9. Arany L, Bhattacharya S, Macdonald JHG, Hogan SJ. Closed form solution of Eigen frequency of monopile supported offshore wind turbines in deeper waters incorporating stiffness of substructure and SSI. *Soil Dynamics and Earthquake Engineering* 2016; **83**: 18–32.
10. Ali A, De Risi R, Sextos A, Goda K, Chang Z. Seismic vulnerability of offshore wind

turbines to pulse and non-pulse records. *Earthquake Engineering & Structural Dynamics* 2020; **49**(1): 24–50.
11. Zhao Z, Dai K, Camara A, Bitsuamlak G, Sheng C. Wind Turbine Tower Failure Modes under Seismic and Wind Loads. *Journal of Performance of Constructed Facilities* 2019; **33**(2): 04019015.
12. Peeters M, Santo G, Degroote J, Van Paepegem W. High-fidelity finite element models of composite wind turbine blades with shell and solid elements. *Composite Structures* 2018; **200**: 521–531.
13. Chen X, Zhao W, Zhao XL, Xu JZ. Preliminary failure investigation of a 52.3m glass/epoxy composite wind turbine blade. *Engineering Failure Analysis* 2014; **44**(11): 345–350.
14. Resor BR. Definition of a 5MW/61.5 m wind turbine blade reference model. *Albuquerque, New Mexico, USA, Sandia National Laboratories, SAND2013-2569 2013* 2013(SAND2013-2569): 53.
15. Berg JC, Resor BR. *Numerical Manufacturing And Design Tool ( NuMAD v2 . 0 ) for Wind Turbine Blades : User ' s Guide*. California: 2012.
16. Navarro-González FJ, Compañ P, Satorre R, Villacampa Y. Numerical determination for solving the symmetric eigenvector problem using genetic algorithm. *Applied Mathematical Modelling* 2016; **40**(7–8): 4935–4947.
17. Holland JH. *Adaptation in natural and artificial systems : an introductory analysis with applications to biology, control, and artificial intelligence*. Michigan: University of Michigan Press; 1975.
18. Goldberg DE. *Genetic algorithms in search, optimization, and machine learning*. California: Addison-Wesley; 1989.
19. Griffith DT, Resor BR. Description of Model Data for SNL100-00 : The Sandia 100-meter All-glass Baseline Wind Turbine Blade.
20. Mishnaevsky L, Branner K, Petersen H, Beauson J, McGugan M, Sørensen B. Materials for Wind Turbine Blades: An Overview. *Materials* 2017; **10**(11): 1285.
21. Manalo A, Aravinthan T, Fam A, Benmokrane B. State-of-the-Art Review on FRP Sandwich Systems for Lightweight Civil Infrastructure. *Journal of Composites for Construction* 2017; **21**(1).
22. MATLAB. *Global Optimization Toolbox User's Guide R2019a*. 2019.
23. McKenna F. OpenSees: a framework for earthquake engineering simulation. *Computing in Science & Engineering* 2011; **13**(4): 58–66.
24. Ali A, De Risi R, Sextos A. Finite element modeling optimization of wind turbine blades from an earthquake engineering perspective. *Engineering Structures* 2020; **222**: 111105.
25. Ali A, De Risi R, Sextos A. Seismic assessment of wind turbines: How crucial is rotor-nacelle-assembly numerical modeling? *Soil Dynamics and Earthquake Engineering* 2021; **141**: 106483.